Simultaneous visualization of spatial and chromatic aberrations by two-dimensional Fourier transform spectral interferometry

W. Amir, T. A. Planchon, C. G. Durfee, and J. A. Squier

Physics, Department of Colorado School of Mines, 1523 Illinois Street, Golden, Colorado 80401

P. Gabolde and R. Trebino

School of Physics, Georgia Institute of Technology, 837 State Street, Atlanta, Georgia 30332

M. Müller

Swammerdam Institute for Life Sciences, University of Amsterdam, 1090 GB Amsterdam, The Netherlands

Received March 27, 2006; revised July 5, 2006; accepted July 11, 2006;
posted July 12, 2006 (Doc. ID 69392); published September 11, 2006

We demonstrate the use of a simple tool to simultaneously visualize and characterize chromatic and spherical aberrations that are present in multiphoton microscopy. Using two-dimensional Fourier transform spectral interferometry, we measured these aberrations, deducing in a single shot spatiotemporal effects in high-numerical-aperture objectives. © 2006 Optical Society of America

OCIS codes: 320.7100, 110.0180.

Image resolution in multiphoton microscopy is a four-dimensional problem. To achieve the highest possible resolution, it is desirable to focus to the smallest possible volume (space) and efficiently excite an optical nonlinearity within this volume (time). This therefore involves the use of high-numerical-aperture (NA) objectives and femtosecond pulses. A consequence of a pulse passing through a refractive optic is the distortion of the femtosecond pulse both spatially and temporally. When propagating through dispersive material, the temporal profile of the ultrashort pulse is broadened and distorted. If this dispersion is uniform across the whole beam, it can be compensated for by a negative dispersion line[1] (prism or grating pair). However, for a multielement imaging system such as that found in microscopy, the difference in glass thickness as a function of pupil position may introduce a radially varying group delay (GD). These are in fact linked to the chromatic and spherical aberration of the refractive optics[2] and are not readily compensated for. Spatial and chromatic aberrations common to most optical systems used in multiphoton imaging deteriorate both the focal volume and the pulse duration.[3,4] In this Letter we characterize the chromatic and spatial aberrations that are involved in multiphoton microscopy by two-dimensional (2D) Fourier transform spectral interferometry. We will restrict the study to the case of on-axis aberrations having cylindrical symmetry by measuring only one direction in the spatial domain.

The first theoretical study on the distortion of a femtosecond pulse due to a refractive lens system was performed by Bor.[5,6] Under the paraxial assumption, he demonstrated that the radially varying GD is equal to the delay between the pulse front and the wavefront and is a result of the chromatic aberration of the lens system. This model was later refined by considering diffraction[4,7] allowing the description of the spatiotemporal pulse near and at focus. Kempe and Rudolph[2,8] improved on this model by considering the spherical aberration that contributes to the radially varying GD. Following their notation, we write the total GD

$$\mathrm{GD}(r) \approx -\pi r^2 + \tau_4 r^4 + \tau_2 r^2. \tag{1}$$

The first term originates from chromatic aberration and is equivalent to the delay between phase front and pulse front given by Bor[5,6] (propagation time delay). The second term arises from the presence of spherical aberration. The last term is due to a defocus term—a delay relative to the paraxial focus plane. The spatial coordinate r is the normalized radial position of the optic; each value of the spatial (radial) coordinate has been divided by the entrance pupil radius of the optic.

To characterize the GD the experimental technique used is 2D spectral interferometry (SI). Bidimensional SI was described by Jaspara and Rudolph.[9] They extracted the delay due to chromatic aberration, but the spherical aberration term was ne-

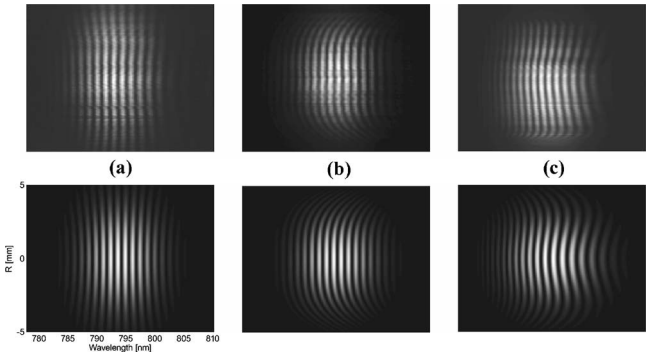

Fig. 1. Experimental (top row) and simulated (bottom row), spectral interferograms with (a) chromatic aberration (b) spherical aberration, and (c) combination of both aberrations.

 © 2006 Optical Society of America

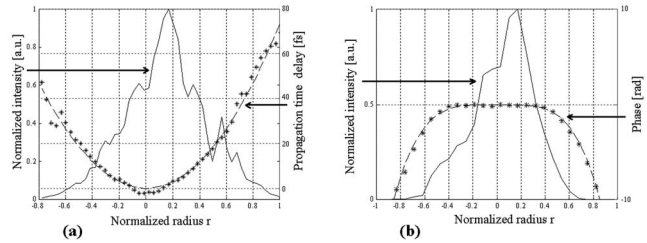

Fig. 2. (a) Propagation time delay (asterisks) extracted from Fig. 1(a) and quadratic fit (dashed curve) giving $\tau = 73.6$ fs. (b) Spatial phase for the central wavelength (asterisks) extracted from Fig. 1(b) and the y^4 fit (dashed curve) ($\tau_2 = 0.93$ fs and $\tau_4 = 13.1$ fs).

glected. Our experimental setup is based on a standard Michelson interferometer followed by an imaging spectrometer.[9] The setup used a 50 fs, 100 mW, 80 MHz Ti:sapphire laser centered at 795 nm. The spectral interferograms recorded are a function of the wavelength λ and beam size r in the transverse direction. The optic to be characterized is placed in the sample arm. To analyze the measured spectral interferogram, the Fourier-transform spectral interferometry method[10] is used. This method begins by taking the Fourier transform of the 2D spectral interferogram and examining the positive frequency component. By taking the inverse Fourier transform of the positive component (generally called the AC portion[11]), the bidimensional amplitude $A(r,\omega)$ and phase $\varphi(r,\omega)$ are extracted.[10–12] The spatiospectral phase[13] given by the optic present in the sample arm is consequently directly extracted in a single shot. To extract the propagation time delay, the derivative of the measured experimental phase $\varphi(r,\omega)$ with respect to ω for each radius is taken at the central frequency ω_0. A quadratic fit of the radially varying propagation time delay results in the parameter τ given in Eq. (1). The 1D spatial phase or wavefront $\varphi(r)$ is a lineout along the r axis of the previous spatiospectral phase at the central wavelength. A polynomial of order 4 fitting the value $[\varphi(r)/\omega_0]$ enables us to extract the parameters τ_2 and τ_4 given in Eq. (1).

By testing simple optics, with well-known aberrations, we validate this tool in terms of measurement and visualization of chromatic and/or spherical aberration. In Fig. 1(a), spectral interferograms for an aspheric microscope objective (New Focus, 20×, 0.5 NA infinity corrected) are shown. This optic primarily produces chromatic aberration. The fringe curvature varies as a function of wavelength, indicating different beam divergence as a function of wavelength. The second optical system, consisting of a parabolic mirror with a thick glass slide (thickness of 0.9 mm), introduces only spherical aberration [see Fig. 1(b)]. The corresponding shape of each fringe, proportional to r^4, is the same for every wavelength. Figure 2(a) shows the propagation time delay for the aspheric objective from Fig. 1(a). The shape is quadratic in r as expected from the spectral interferogram exhibiting chromatic aberration. In Fig. 2(b), the phase at the central wavelength is plotted in the case of the parabolic mirror with the glass, showing the r^4 behavior characteristic of spherical aberration. When the sample-arm mirror is increased slightly in length, a defocus term $\tau_2 r^2$ is added and can be extracted from the interferogram without changing the value of the spherical aberration. In Fig. 2(b), no defocus term is seen, as we were at the paraxial focus of the parabolic mirror ($\tau_2 = 0$).

Complex systems such as multielement, high-NA microscope objectives were also studied. Figure 1(c) shows a spectral interferogram from a 100×, 1.25 NA oil-immersion microscope objective (Zeiss, corrected for a tube length of 160 mm). The interferogram indicates a combination of spherical and chromatic aberrations. The microscope objective was used without the associated tube lens in our collimated light system, which may account for some of the spherical and chromatic aberration observed in the measurements. Notably, this objective is optimized for use in the visible spectrum, not the near-IR. Simulated spectral interferograms have the same fringe structures shown in the experimental interferogram in Fig. 1. The simulations were performed by adding a spatiospectral phase term to the field in the sample arm (e.g., for spherical aberration this is a phase term that scales with the fourth order of the entrance pupil radius).

Figure 3(a) presents the 2D phase for the high-NA oil objective from Fig. 1(c). The shape of the spatiospectral phase varies from a quartic shape (at lower wavelengths) to a saddle-type shape (at longer wavelengths). Figure 3(b) shows, for the high-NA oil objective, the delays deduced from the spatiospectral phase. The delay due to spherical aberration (crosses) is fitted by a polynomial and gives the coefficients τ_4 and τ_2. A fit of the propagation time delay (triangles) gives the coefficient τ. The total delay [see Eq. (1)], sometimes called the radially varying time of flight, is then the sum of the two previous delays. On the edge of the optic, the spherical aberration adds a delay that is not negligible. It increases the GD by around 30%.

Table 1 presents a summary of coefficients τ, τ_4, and τ_2 for the previous optics. The most commonly used spherical aberration coefficient A, linked to τ_4 by the relation[2] $\tau_4 = 3A/\omega_0$, is also shown. Notice that

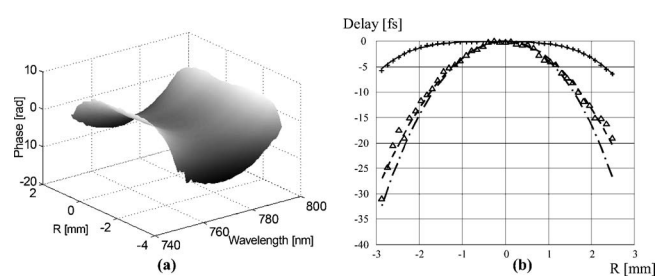

Fig. 3. Oil-immersion objective of Fig. 1(c): (a) experimental spatiospectral phase and (b) radial delay. In (b), the crosses are the delay from the 1D phase lineout at the central wavelength, and the polynomial fit is shown by the solid curve, giving $\tau_2 = 2.2$ fs and $\tau_4 = 9.2$ fs. The triangles are the propagation time delay, and the quadratic fit is shown by the dashed curve, giving $\tau = 49.6$ fs. The dashed–dotted curve is the sum of both fits, representing the total GD.

Table 1. Summary of the Coefficients Representing Chromatic Aberration (τ), Spherical Aberration (τ_4), and the Defocus Term (τ_2) for Different Optics

Optics Element	τ (fs)	τ_2 (fs)[b]	τ_4 (fs)	A
Empty interferometer	0.3	0.02	0.06	0.05
Parabolic mirror (f=12 mm, EPR[a] =6 mm)				
(Paraxial plane)	–	0.93	13.1	10.3
(Best focus)	–	−11.1	12.6	9.9
Aspheric lens (20×, 0.5-NA, EPR = 4 mm)	73.6	0.6	1.1	0.8
Oil objective Zeiss (100×, 1.25-NA, EPR = 3.5 mm)				
(Paraxial plane)	49.6	2.2	9.2	7.2
(Best focus)	53.4	−8.3	10.1	7.9

[a]Entrance pupil radius.

[b]The position of the refractive optics at the paraxial plane was determined visually by obtaining straight fringes near the optical axis. The determination of the paraxial plane is then approximate and explains why the value of τ_2 is not always exactly equal to 0 in the paraxial plane.

at best focus the defocus term decreases the amount of spatial aberration by having the opposite sign to the spherical aberration, as expected. The chromatic and spherical aberrations are virtually identical for the best focus and the paraxial cases. The resolution of our method is estimated by the experimental measurement of the empty interferometer shown in Table 1 and the precision of our fits, which gives a relative error of ±3% in the determination of the coefficients.

To study the effects of these aberrations on the pulse duration at focus, we have to consider which microscope objective is used. When there is no spherical aberration as with the aspheric objective, the pulse broadening is dominated by the chromatic aberration. By integrating the local pulse duration, and taking into account the GD(r) as in Ref. 14, we can estimate the pulse duration at focus. For a 25 fs input pulse duration (and using a Gaussian beam with FHWM equal to the clear aperture of the objective), the pulse duration is increased to 35 fs. For an input pulse of 100 fs, the effect is less severe, resulting in a broadened pulse at focus of 102 fs. When an objective combining both chromatic and spherical aberrations is used, we have to study two limiting cases, depending on the initial pulse duration. The parameter used to evaluate whether spherical aberration is dominant is A_2, given in Ref. 2. When A is greater than A_2, the spherical aberration is dominant and the in-focus duration is not broadened.[2] When A is much smaller than A_2, the chromatic aberration is dominant and the pulse duration is increased. As an illustration of these two limiting cases, we will take τ=25 fs and A =5, which are reasonable values for a high-NA objective after one pass through the objective (see Table 1 for the two-pass values). For input pulse durations greater than 15 fs, spherical aberration is dominant ($A > A_2$). This means that these pulses will essentially not be affected by an increase in duration at focus. Nevertheless, the spatial resolution decreases because of the presence of spherical aberration. When we use a pulse shorter than 15 fs, the effect of chromatic aberration will become more important and the pulse duration will be broadened at focus to almost 25 fs (value of τ). Thus these measurements, for these optics, demonstrate that for the typical multiphoton microscopist utilizing pulse widths of the order of 50 fs or greater, these effects are negligible.

In conclusion, we have demonstrated a simple technique for characterizing the complex spatial and temporal behavior of ultrashort pulses focused by high-NA objectives. We observed in a single spectral interferogram the chromatic and spherical aberrations very clearly, allowing us to study the influence of these aberrations on the spatially varying group delay and showing that the effect of spherical aberration is not negligible. This method is applicable to any complex imaging system incorporating ultrashort pulses. Notably, due to the linearity of this technique, it requires extremely small amounts of light. It can therefore be readily multiplexed into a multiphoton imaging system to measure distortions as a function of sample depth, for instance. This information can in principle be actively fed back and used to correct, at least in terms of the spherical aberration.

This work was partially supported by the National Science Foundation (NSF) Division of Earth Sciences, EAR 0337379, and by grant EB003832 through the National Institute of Biomedical Imaging and Bio Engineering. R. Trebino acknowledges support from the NSF (grant ECS-0200223). W. Amir's e-mail address is wamir@mines.edu.

References

1. J. A. Squier and M. Müller, Rev. Sci. Instrum. **72**, 2855 (2001).
2. M. Kempe and W. Rudolph, Phys. Rev. A **48**, 4721 (1993).
3. C. J. R. Sheppard and T. Wilson, Appl. Opt. **18**, 1058 (1979).
4. M. Kempe, U. Stamm, B. Wilelml, and W. Rudolph, J. Opt. Soc. Am. B **9**, 1158 (1992).
5. Z. Bor, Opt. Lett. **14**, 119 (1989).
6. Z. Bor, J. Mol. Spectrosc. **35**, 1907 (1988).
7. Z. Bor and R. L. Horvath, Opt. Commun. **94**, 249 (1992).
8. M. Kempe and W. Rudolph, Opt. Lett. **18**, 137 (1993).
9. J. Jasapara and W. Rudolph, Opt. Lett. **24**, 777 (1999).
10. L. Lepetit, G. Chériaux, and M. Joffre, J. Opt. Soc. Am. B **12**, 2467 (1995).
11. C. Iaconis and I. A. Walmsley, IEEE J. Quantum Electron. **35**, 501 (1999).
12. R. Trebino and D. J. Kane, J. Opt. Soc. Am. A **10**, 1101 (1993).
13. C. Dorrer, E. M. Kosik, and I. A. Walmsley, Opt. Lett. **27**, 548 (2002).
14. T. A. Planchon, S. Ferré, G. Hamoniaux, G. Cheriaux, and J.-P. Chambaret, Opt. Lett. **29**, 2300 (2004).